https://doi.org/10.15255/KUI.2026.003
KUI-36/2026
Original scientific paper
Received February 3, 2026
Accepted April 3, 2026

Chemically Modified Pine Bark as a Sustainable and Low-Cost Biosorbent for Efficient Th(IV) Removal from Water: Characterisation, Kinetic, Isotherm, and Thermodynamic Studies

J. M. Aljaafreh,[a] *F. I. Khalili*,[b] *M. S. Mousa*,[c] *O. A. Alnasra*,[d] *D. Sobola*,[e] *G.-Z. Zhu*,[f] *K. Lisichkov*,[g] *T. Kitanovski*,[g]* *A. M. D. A. Jaber*,[h] *Z. M. Alqudah*,[i] and *A. M. Abuamr*[f]

[a] Department of Physics, School of Science, The University of Jordan, Amman, Jordan
[b] Department of Chemistry, School of Science, The University of Jordan, Amman, Jordan
[c] Department of Renewable Energy Engineering, Jadara University, Irbid 21 110, Jordan
[d] Department of Chemistry, School of Science, Jerash Private University, Jerash, Jordan
[e] Department of Physics, Faculty of Electrical Engineering and Communication, Brno, University of Technology, 61 600 Brno, Czech Republic
[f] Department of Mechanical Engineering and Manitoba Institute for Materials, University of Manitoba, Winnipeg, MB R3T 5V6, Canada
[g] Faculty of Technology and Metallurgy Skopje, Ss. Cyril and Methodius University in Skopje, Ruger Boskovic 16, 1000 Skopje, N. Macedonia
[h] Department of Basic Humanities and Sciences, Faculty of Medicine, Aqaba Medical Sciences University, Aqaba 77 110, Jordan
[i] Jordan Atomic Energy Commission, Amman 11 934, Jordan

Abstract

The adsorption behaviour of thorium (Th(IV)) ions on modified pine bark (MPB) was systematically investigated with respect to pH, adsorbent dosage, temperature, and contact time. Kinetic evaluation using the pseudo-second-order (PSO) model indicated that the equilibrium adsorption capacity (q_e) of MPB, measured at pH 3, achieved a maximum uptake of approximately 90 %, with a q_e value of 12.97 mg g^{-1} at 25 °C. Adsorption isotherm analysis was conducted utilising Langmuir, Freundlich, and Dubinin–Radushkevich models.

The Langmuir model showed a better correlation (R^2) than the Freundlich model, suggesting monolayer adsorption with a degree of surface heterogeneity. Thermodynamic parameters, including enthalpy ($\Delta H°$), entropy ($\Delta S°$), and Gibbs free energy ($\Delta G°$), were calculated at different temperatures. At 25 °C, the thermodynamic values were $\Delta H° = 83.10$ kJ mol^{-1}, $\Delta G° = -6.58$ kJ mol^{-1}, and $\Delta S° = 301.18$ J mol^{-1} K^{-1}. These results confirm that adsorption was spontaneous and endothermic, with an increase in entropy. Overall, MPB exhibited significant potential as an effective adsorbent for the removal of Th(IV) ions from aqueous solutions.

Keywords

Adsorption, isotherm modelling, pine bark, modified pine bark, thorium

1 Introduction

Environmental pollution caused by heavy metals, including Th(IV), has become a critical global concern due to its toxic and radioactive nature.[1] Th(IV) contamination originates from mining activities, nuclear operations, and various industrial processes, posing serious risks to ecosystems and human health.[2] Various treatment methods have been developed for the removal of such contaminants, as presented in Table 1. Consequently, the search for low-cost, sustainable, and efficient adsorbents[3] for Th(IV) removal has gained significant attention.[4] Adsorption is considered one of the most efficient and practical methods for treating industrial wastewater due to its high efficiency, low cost, ease of regeneration, and the absence of sludge generation. It has been widely applied for the removal of radioactive elements from hazardous effluents.[5]

Biosorption using natural and modified biomass has emerged as a viable alternative for heavy metals removal.[11] Among various biosorbents, pine bark, a lignocellulosic by-product of the timber industry, has shown considerable potential due to its abundance, low cost, and rich polyphenolic composition. These polyphenolic compounds contain functional groups, such as hydroxyl and carboxyl groups,[12,13] which can effectively chelate metal ions. Despite its favourable properties, raw pine bark exhibits limited adsorption capacity and selectivity, thereby necessitating chemical modification to enhance its efficiency.[14,15]

Previous studies have demonstrated the successful application of modified pine bark for the removal of heavy metals such as cadmium, lead, and chromium.[16] Table 2 presents

* Corresponding author: Tome Kitanovski, M.Sc. Tech.
Email: tome_kit22@yahoo.com

Table 1 – Comparison of water purification methods: strengths, limitations, and current insights

Ref.	Method	Benefits	Limitations
6	Coagulation and flocculation	With appropriate chemical dosing, high removal efficiency can be achieved	Produces large amounts of sludge requiring treatment; energy-intensive; high operating costs
7	Ion exchange	Effective at eliminating both cations and anions; performs efficiently at low pressure	High resin cost; susceptible to oxidation; expensive disposal of regenerant chemicals
8	Membrane filtration	Effective at low temperatures without phase change	Membrane fouling; expensive cleaning and maintenance; shear stress may damage sensitive chemical compounds
9	Photocatalysis	Produces less hazardous by-products; high photostability	Slow degradation rate; limited scalability in real-world systems
10	Chemical precipitation	High selectivity enables removal of specific ions while preserving the presence of others	Produces large amounts of sludge/salt; high operating costs

Table 2 – WHO and EPA standards for toxic heavy metals and corresponding health implications

Sr.	Heavy metal	WHO limit / $mg\,l^{-1}$	EPA MCL / ppb[a]	Industry range / $mg\,l^{-1}$	Permissible limit / $mg\,l^{-1}$	Adverse health effects
1	Nickel (Ni)	0.07	–	0.5–1000	5.0	Skin/lung damage, cardiovascular issues
2	Silver (Ag)	0.1	–	–	–	Blood cell issues, liver/kidney dysfunction
3	Copper (Cu)	–	1300	–	–	Gastrointestinal distress
4	Iron (Fe)	3.0	–	–	–	Hemochromatosis, liver cell damage
5	Cadmium (Cd)	0.003	5	0.1–22	0.5	Immune system damage, osteomalacia, anaemia
6	Arsenic (As)	0.05	10	0.01–1.0	0.01	Skin lesions, cancer, liver cirrhosis, mental disorders
7	Chromium (Cr)	0.05	100	0.01–1.5	0.1	Eczema, genotoxicity, lung
8	Cobalt (Co)	0.05	–	–	–	Asthma, allergic reactions, bronchitis, possible cancer
9	Lead (Pb)	0.05	15	5–700	2.0	Neurotoxicity, kidney issues, Alzheimer's, cancer
10	Zinc (Zn)	3.0	–	0.3–5	5.0	Respiratory disease, neurological effects
11	Mercury (Hg)	0.1	2	0.05–2.5	0.1	Kidney damage, hypertension, neurological disorders
12	Uranium (U)	0.03	30	0.01–2.0	0.03	Kidney toxicity, increased cancer risk
13	Thorium (Th)	–	–	0.005-0.5	0.015	Bone cancer, liver damage, radiotoxicity

MCL: maximum contaminant level, 1 ppb = 1 $\mu g\,l^{-1}$, ppb: parts *per* billion[21]

the regulatory limits for these metals, providing a detailed comparison of toxic heavy metals based on the standards set by the World Health Organization (WHO) and the Environmental Protection Agency (EPA). However, research on the potential of Th(IV) adsorption remains limited in the literature. Chemical modifications, including acid or base treatments,[17] oxidation processes, and functional group grafting,[18,19] have been employed to improve the adsorption characteristics of pine bark. These modifications enhance the active binding sites, increase the surface area, and improve the affinity of thorium ions toward the surface of the materials.[20]

The present study aims to investigate the feasibility of using chemically modified pine bark as an adsorbent for the removal of Th(IV) ions from water, and to assess the effect of chemical modification on its adsorption efficiency. The operational mechanism of this research is further illustrated in the schematic representation provided in Fig. 1.

2 Experimental

2.1 Materials

The bark of *Pinus* (pine bark) obtained from Alyobeel Forest (Jordan) was used in this study. All chemicals used were of analytical grade and applied without further purification. Arsenazo(III) and thorium (IV) nitrate tetrahydrate were

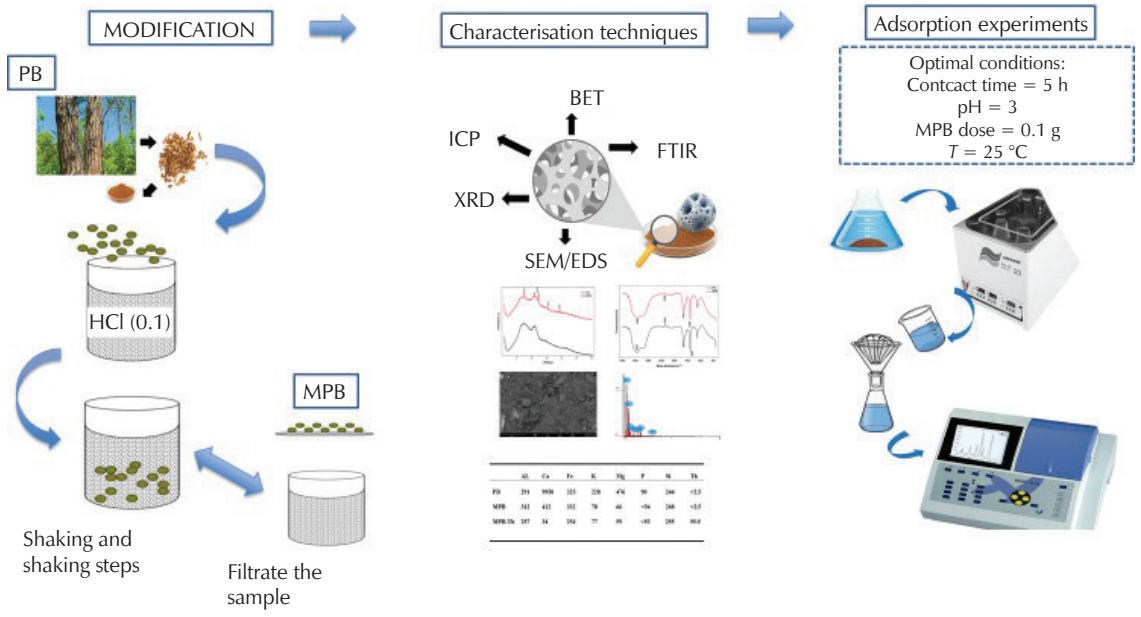

Fig. 1 – Stepwise illustration of pine bark modification, characterisation, and adsorption experiments

provided by Janssen Chimica. Hydrochloric acid (37 %, HCl) was sourced from S&C Supplico Chemical, while sodium hydroxide (NaOH) pellets were obtained from SDS Vorte Partenaire Chimie.

2.2 Instruments

Weighing was carried out using an analytical balance (RADWAG® AS 220 R2). The pH measurements were performed using a pHS-250 microprocessor pH-meter (BANTE instruments). Fourier transform infrared (FTIR) spectra were recorded using a Thermo Nicolet NEXUS 670 spectrophotometer. Crystalline phases were identified by X-ray diffraction (XRD) using a Philips X'pert PW 3060 diffractometer, Cu Kα radiation source, operating at 40 mA and 45 kV. A Phenom XL G2 scanning electron microscope SEM combined with an EDS detector; accelerating voltage of 15 kV and a pressure of $6 \cdot 10^{-4}$ Pa.

Adsorption experiments were conducted under controlled agitation using a thermostatic shaker (model IN-666). Metal ion concentrations were determined using a visible spectrophotometer (METASH V-5100). The specific surface area and pore structure were analysed using the Brunauer–Emmett–Teller (BET) method with a Quantachrome® ASiQwin™ automated gas sorption system. Inductively coupled plasma optical emission spectroscopy (ICP-OES) was performed using a Thermo Scientific iCAP 7200, with argon as the cooling gas, an external chiller for cooling, dual plasma viewing, and a radiofrequency generator: 27 MHz solid-state, optimised at ~1150 W (range 750–1500 W). Inductively coupled plasma mass spectrometry (ICP-MS) was performed using a Thermo Scientific iCAP RQ with argon as the cooling gas, an external chiller for cooling, and a radiofrequency generator: Digital solid-state ~27 MHz (hot plasma at 1550 W).

2.3 Preparation and modification of adsorbents

The pine bark was ground, sieved, and dried in an oven at 80–85 °C for 2 h. Modification was performed in an acidic medium using hydrochloric acid.[14] A total of 25 g of pine bark was added to 500 ml of 1 M HCl in a conical flask and stirred at 200 rpm for 2.5 h. The solution was filtered and repeatedly washed with distilled water, and subsequently dried in an oven at 80 °C for 2 h.[16]

2.4 Adsorption of Th(IV)

The effects of various factors, including pH, initial thorium concentration, contact time, temperature, and adsorbent dosage, were investigated using a batch technique.[22] Each experiment was conducted in a 100 ml vessel containing 25 ml of Th(IV) solution maintained under constant agitation.[23,24] After adsorption, the samples were filtered using Whatman No. 42 filter paper. The concentration of residual thorium ions in each sample was determined spectrophotometrically at a wavelength of 660 nm using Arsenazo(III). Optimised parameter values (concentration = 50 mg l^{-1}, pH = 3, and mass = 0.1 g) were applied in subsequent experiments.[25]

The adsorption capacity (q_e) and removal efficiency (R) were determined using Eqs. (1)–(2):

$$q_e = \frac{(c_i - c_e)}{w} \cdot V \tag{1}$$

$$R = \frac{(c_i - c_e)}{c_i} \cdot 100 \tag{2}$$

where c_i is the initial thorium concentration in mg l^{-1}; c_e is the residual thorium concentration (mg l^{-1}); w is the mass of MPB in grams; and V is the solution volume (L).[26]

3 Results and discussion

3.1 Chemical composition

Pine bark is a lignocellulosic biomass composed primarily of cellulose (20–35 %), hemicellulose (10–25 %), and lignin (20–40 %). It also contains smaller amounts of extractives, including tannins, polyphenols, resins, and inorganic ash components.[27] These components consist of a variety of functional groups, including phenolic groups, carboxyl (−COOH), and hydroxyl (−OH), which contribute to its adsorption potential.[28] In a batch modification system, hydrochloric acid (HCl) treatment facilitates the removal of loosely bound inorganic ions (*e.g.*, Ca^{2+}, K^{+}, Na^{+}) through ion exchange with protons (H^{+}) and promotes hydrolysis of the ester linkage, generating additional carboxylic and phenolic groups. This process enhances surface area and pore accessibility.[29]

Acid treatment also promotes partial hydrolysis of hemicellulose and alters lignin structure, consequently increasing the availability of active adsorption sites. Furthermore, HCl can help clean the surface of impurities, increase the proportion of active surfaces, and remove water-soluble tannin compounds that may impart a brown colour and interfere with the adsorption experiments and colourimetric measurements.[30] The chemical reactions in the solution can be described by the following Eqs. (3)–(4):

$$4Ar\text{–}COO - H + Th^{4+} \rightarrow (Ar - COO)_4\ Th + 4H^{+} \quad (3)$$

$$4(Ar - O - H) + Th^{4+} \rightarrow (Ar - O)_4\ Th + 4H^{+} \quad (4)$$

where Ar represents the functional groups of bark, including lignin and polysaccharides.

3.2 Characterisation

3.2.1 Fourier transform infrared (FTIR) analysis

Fig. 2 presents the FTIR analysis of natural pine bark (PB) and HCl-modified pine bark (MPB). A broad absorption band measuring 3200–3700 cm^{-1}, corresponding to the stretching of hydroxyl O−H groups present in hemicellulose, cellulose, and lignin, appears at 3380 cm^{-1} for PB and shifts to 3436 cm^{-1} in MPB, indicating changes in hydrogen bonding due to acid hydrolysis.[31] Both samples exhibit a band at 2358 cm^{-1}, potentially associated with residual CO_2 adsorbed on the biomass surface.

A prominent peak at around 1637 cm^{-1} in PB and 1635 cm^{-1} in MPB corresponds to aromatic C=C stretching as well as C=O stretching of linked carbonyl groups, suggesting that the aromatic framework remained largely unaltered after modification[32]. The band at 1385 cm^{-1}, seen in both spectra, corresponds to phenolic O−H bending and aliphatic CH deformation, indicating the retention of both groups.[28]

A slight shift in the C−O stretching vibration from 1107 cm^{-1} in PB to 1110 cm^{-1} in MPB indicates structural changes within the polysaccharide matrix, likely due to hemicellulose hydrolysis.[33,34] Overall, the spectra confirm the presence of essential lignocellulosic constituents in both samples, and the alterations found after HCl treatment suggest increased accessibility of active functional groups, potentially enhancing the material's capacity for adsorbing heavy metals in acidic environments.

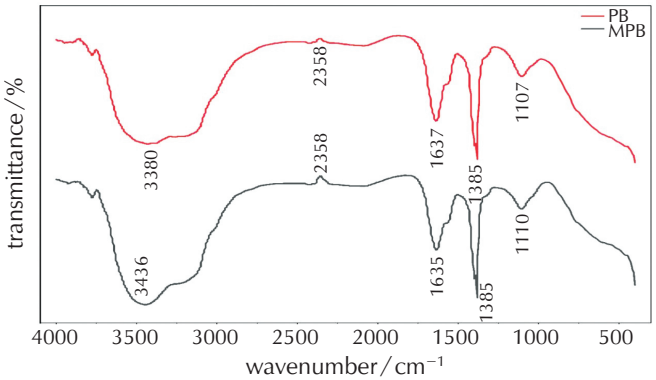

Fig. 2 – FTIR spectra of PB and MPB

3.2.2 X-ray diffraction XRD analysis

Fig. 3 presents the XRD patterns of natural pine bark (PB) and HCl-modified pine bark (MPB), illustrating the structural changes resulting from acid treatment.[35] The diffraction pattern of PB exhibits multiple broad peaks with distinct maximum values at 2θ close to 15.1°, 22.0°, and 24.6°. These peaks correspond to the partially organised structure of lignocellulosic biomass, particularly the organised regions of cellulose.[36]

The peak observed at 22.0° is generally attributed to the (002) lattice plane of cellulose, indicating the presence of both crystalline and amorphous cellulose structures.[37] The additional peaks observed at 30.3° and 38.4° may be attributed to trace minerals or structural organisation of organic matter within the biomass.[38] The MPB pattern exhibits a broad, less intense profile characterised by reduced peaks, indicating a significant reduction in crystallinity.[12]

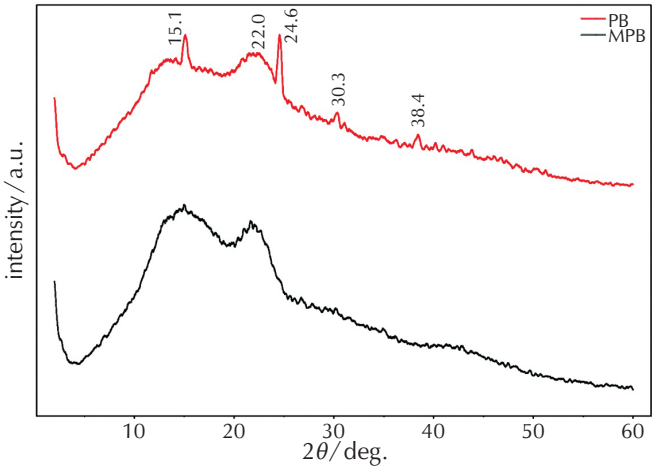

Fig. 3 – XRD spectra of PB and MPB

The attenuation of the peaks in the MPB sample indicates that the cellulose structure had been altered and transformed into a more amorphous state due to hydrolysis by hydrochloric acid. The observed reduction in peak sharpness and intensity indicates the synthesis of polysaccharide chains and the potential removal of less organised lignin and hemicellulose components, which is commonly observed in the lignocellulosic materials subjected to acid treatment.

The XRD results confirm that HCl treatment modified the structure of pine bark, reducing its crystallinity and enhancing its amorphous characteristics. This modification may facilitate improved adsorption by increasing surface area and providing easier access to active sites.

3.2.3 BET surface analysis

The N_2 adsorption-desorption isotherms of PB and MPB reveal notable differences in their textural properties, as listed in Table 3.[39] The specific surface area of MPB (8.045 $m^2 g^{-1}$) was nearly double that of PB (4.374 $m^2 g^{-1}$), indicating a substantial enhancement in surface characteristics following acid modification.[38] This increase in surface area suggests the generation of additional active sites, which is critical for adsorption efficiency.[40]

Furthermore, a slight reduction in average pore size from 4.678 nm (PB) to 4.367 nm (MPB) was observed, implying an increase in pore density and accounts for the observed increase in total pore volume from 0.007 to 0.010 cc g^{-1}.[12] These findings align closely with data published in the literature,[41] and confirm the effectiveness of the modification process in improving the adsorptive potential of lignocellulosic biosorbents.

Table 3 – Pore size, surface area, and pore volume analysis of PB and MPB *via* DFT

Adsorbent	Pore size / nm	Surface area / $m^2 g^{-1}$	Pore volume / cc g^{-1}	Ref.
PB	4.678	4.374	0.007	this work
MPB	4.367	8.045	0.010	this work
PB	–	4.95	0.01	41
MPB	–	8.74	0.04	41

3.2.4 SEM-EDX analysis

Fig. 4 presents SEM micrographs together with the corresponding EDX elemental spectra of PB and MPB. The surface morphology of both materials exhibited a heterogeneous and fibrous structure, characterised by irregular, shallow pores and dense clusters, which are typical of lignocellulosic biomass.[42] EDX analysis confirms these findings, indicating that both PB and MPB are composed predominantly of carbon and oxygen, consistent with their lignocellulosic nature.[43] In PB, the atomic concentrations of carbon and oxygen were 62.64 and 28.23 %, respectively.

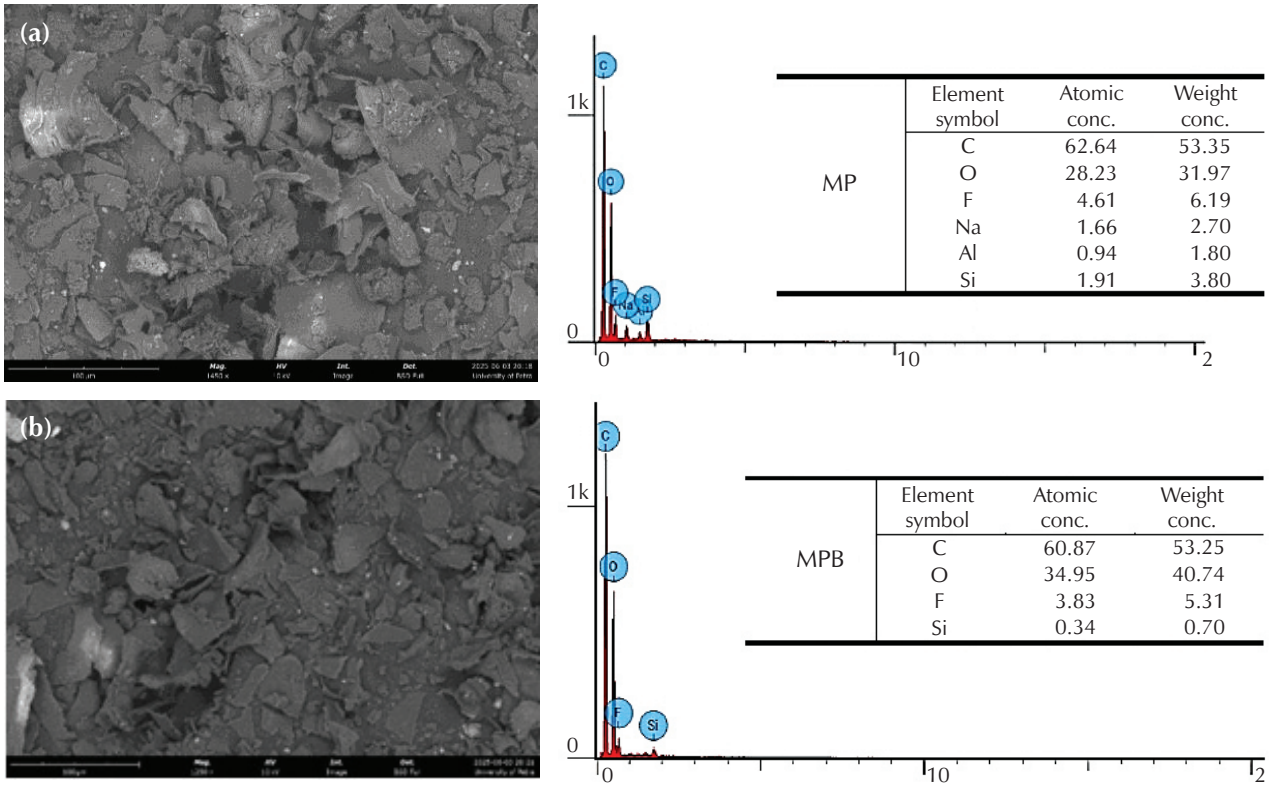

	Element symbol	Atomic conc.	Weight conc.
MP	C	62.64	53.35
	O	28.23	31.97
	F	4.61	6.19
	Na	1.66	2.70
	Al	0.94	1.80
	Si	1.91	3.80

	Element symbol	Atomic conc.	Weight conc.
MPB	C	60.87	53.25
	O	34.95	40.74
	F	3.83	5.31
	Si	0.34	0.70

Fig. 4 – SEM images and EDX spectra of (a) PB and (b) MPB

Minor elements detected included fluorine (4.61 %), sodium (1.66 %), aluminium (0.94 %), and silicon (1.91 %). In the MPB sample, the carbon content decreased to 60.87 %, while the oxygen content increased to 34.95 %, indicating changes in surface composition, likely due to the leaching of inorganic components and hydrolysis of ester linkages, resulting in greater exposure of oxygen-containing functional groups.

Fluorine and silicon remained present at lower concentrations (3.83 and 0.34 %, respectively), whereas sodium and aluminium were largely removed, demonstrating the leaching effect of HCl treatment.

The elevated oxygen content, together with improved surface smoothness, indicate that HCl treatment enhanced surface functionality and porosity, likely via partial degradation of the lignin matrix and the exposure of additional active functional groups. The observed morphological and elemental changes are consistent with the increase in pore volume observed in the BET analysis (Table 3),[44] thereby confirming the effectiveness of chemical modification in enhancing the adsorption potential of MPB.[45]

3.2.5 ICP-OES and ICP-MS analysis

Table 4 presents the ICP-OES analysis of pine bark PB and modified pine bark MPB before and after thorium adsorption, showing a substantial decrease in the concentrations of various elements at each experimental stage.[46] The highest elemental values were observed in raw PB, followed by a reduction after chemical modification with hydrochloric acid, and a further decrease after thorium adsorption. This reduction is attributed to the ionisation and leaching of elements during the modification and adsorption processes.[47] To specifically quantify thorium, ICP-MS analysis was employed. The results indicate that thorium was below the detection limit (< 2.5 mg kg^{-1}) in both PB and MPB prior to exposure. However, after adsorption, thorium concentration in MPB–Th increased significantly to 55.5 mg kg^{-1}; confirming the effective uptake of Th(IV) ions by the modified adsorbent.[48,49]

Table 4 – ICP–OES and ICP-MS elemental analysis of PB, MPB, and MPB-Th in mg kg^{-1}

	Ca	Mg	Fe	Al	K	P	Si	Th
PB	9950	476	325	291	228	90	244	<2.5
MPB	412	66	332	312	78	54	268	<2.5
MPB-Th	34	59	254	257	77	53	255	55.5

3.3 pH effect

Fig. 5 shows that the adsorption rate was relatively low under acidic conditions, as the high concentration of H^+ ions dominated the solution and prevented the attachment of thorium ions to the active sites on the adsorbent surface. As the pH increased, the adsorption capacity also increased. At pH values above 5, hydrolysis of thorium ions may occur, leading to the formation of insoluble hydroxide($Th(OH)_4$) species.[50] These precipitates may settle out of solution (Fig. 6), giving a misleading indication of increased adsorption. Therefore, a pH of 3 was selected as the optimal condition for thorium uptake, as hydrolysis is minimal, and the metal ions remain soluble and available for adsorption, and this is mainly due to surface adsorption.[5]

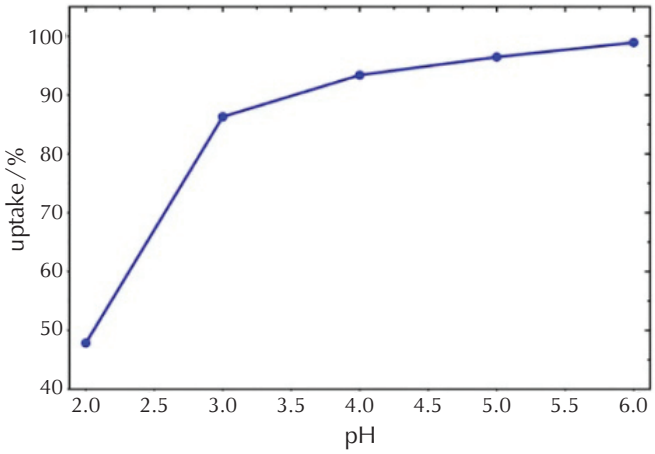

Fig. 5 – Effect of pH on the uptake (%) of Th(IV) ions by MPB

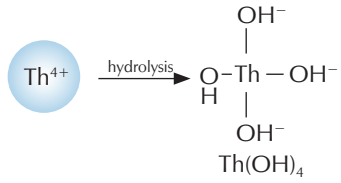

Fig. 6 – Schematic representation of Th(IV) hydrolysis and precipitation at pH > 5

3.4 Effect of adsorbent dosage

The amount of adsorbent has a significant influence on adsorption behaviour. As the adsorbent dose increases, the removal efficiency increases significantly due to the greater availability of active sites for metal ion interaction.[22] Fig. 7 shows that the adsorption uptake increased significantly from 71.2 to 98.6 % as the adsorbent dose was raised from 0.025 to 0.2 g. This observation confirms that increasing the adsorbent dosage enhances the removal of metal ions from water.[23]

3.5 Contact time effect

Fig. 8 presents the relationship between contact time and the adsorption efficiency of Th(IV) ions onto MPB. A rapid increase in adsorption was observed during the initial stages of the process, with over 55 % of Th ions adsorbed during the first hour.[5] The uptake then increased

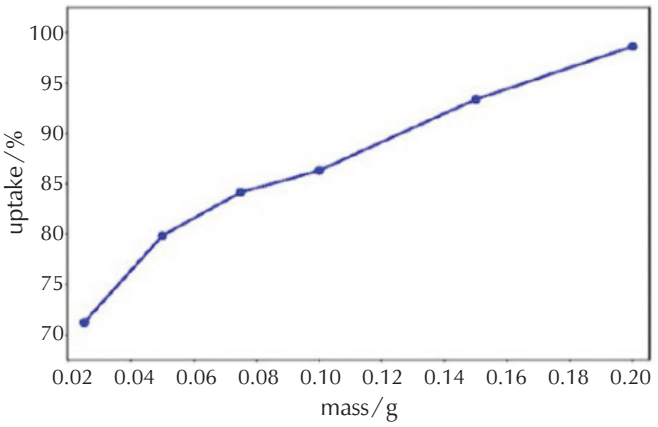

Fig. 7 – Effect of adsorbent dosage on the removal efficiency (%) of Th(IV) ions using modified pine bark (MPB)

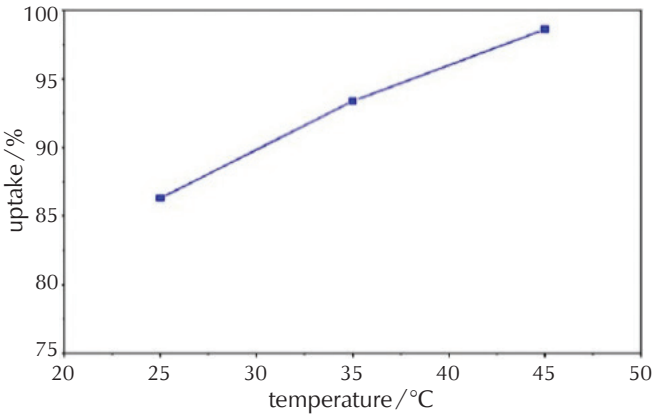

Fig. 9 – Effect of temperature on Th(IV) adsorption using MPB

to 81 % after 2 h. Beyond this stage, the adsorption rate stabilised, signifying a gradual attainment of equilibrium. The adsorption equilibrium was reached at almost 5 h, indicating that this is the equilibrium contact duration.[51] Upon achieving equilibrium, no notable alteration in adsorption capacity was detected. The equilibrium stage was reached when the surface active sites of MPB were saturated and the adsorption and desorption rates became balanced.[52]

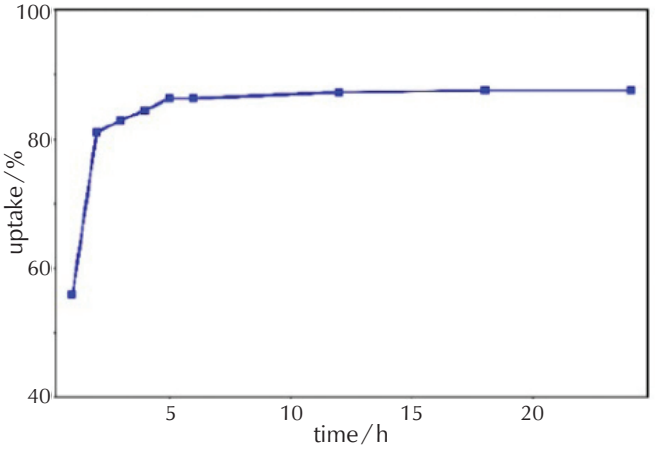

Fig. 8 – Effect of contact time on the adsorption (%) of Th(IV) ions onto modified pine bark (MPB)

3.6 Temperature effect

Fig. 9 shows the influence of temperature on Th(IV) ion removal using MPB. The increase in temperature from 25 to 45 °C resulted in an increase in uptake efficiency from 86 to 98 %. This increase indicates endothermic adsorption.[53] The observed increase suggests that high temperatures increase the mobility of Th(IV) ions, which enhances the interaction between the adsorbent surface sites and the adsorbate, leading to increased uptake.[32]

3.7 Sorption kinetics

Sorption kinetics provide important details about the rate of ion adsorption, serving as an essential factor in the assessment of the overall adsorption process. The adsorption kinetics were determined using the pseudo-first and second order models.[25] The linearised representation of the pseudo-first-order (PFO) equation:

$$\ln(q_e - q_t) = \ln(q_e) - k_1 \tag{5}$$

where q_e and q_t are adsorption capacities at equilibrium, e, and time, t (mg g^{-1}), respectively, k_1 is the PFO rate constant (min^{-1}). A linear plot of $\ln(q_e - q_t)$ *vs.* t (Fig. 10(a)) allows determination of k_1.[54]

Similarly, the pseudo-second-order (PSO) kinetic model is expressed as:

$$\frac{t}{q_t} = \frac{1}{k_2 q_e^2} + \frac{t}{q_e} \tag{6}$$

The PSO rate constant (k_2, g/mg/min), equilibrium adsorption capacity (q_e, mg g^{-1}), and the adsorbate amount at time t (q_t, mg g^{-1}) were derived by plot of t/q versus t, as shown in Fig. 10(b). The slope and intercept of this line enable the calculation of the values of q_e and k_2.[55] The calculated q_e was eventually compared with the experimental values to evaluate the fitness of the model.[56]

Table 5 presents the kinetic parameters for Th(IV) ions adsorption on MPB, assessed by PFO and PSO models. The PSO model exhibited a superior fit to the experimental data, indicated by the higher regression coefficient (R^2 = 0.99) in comparison with the PFO model (R^2 = 0.93). Furthermore, the determined equilibrium adsorption capacity (q_e) from PSO model (10.99 **mg** g^{-1}) matched closely with the experimental value (10.94), but the q_e derived from the PFO model was considerably lower (1.25 mg g^{-1}), signifying insufficient model precision. The tendency is consistent when compared to previous studies on other metal ions. In almost all instances, the PSO model demonstrated excellent R^2 values (between 0.93 and 0.99), thereby validat-

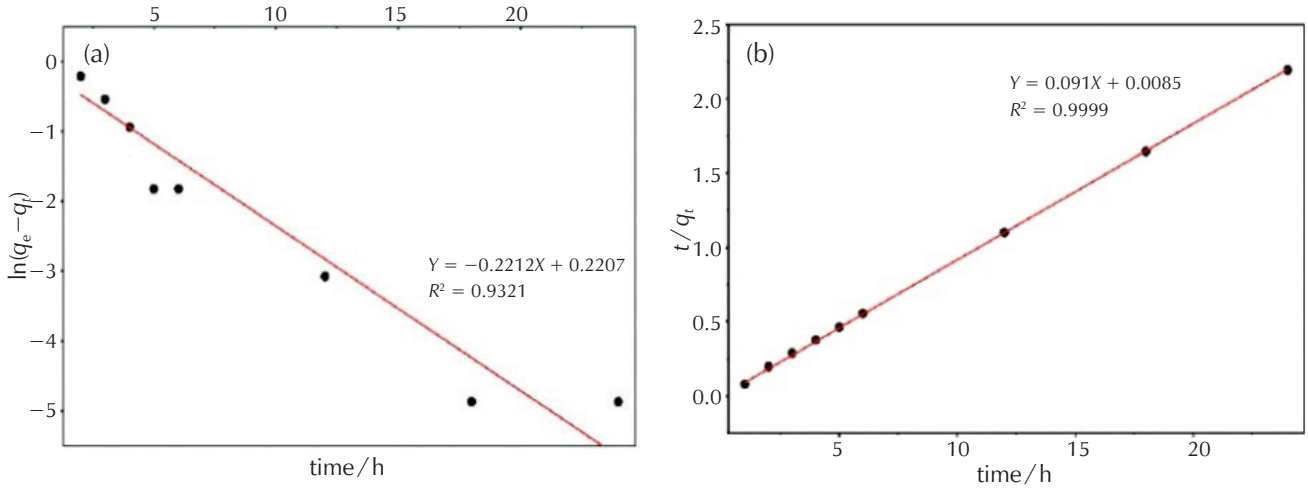

Fig. 10 – Kinetic models for Th(IV) adsorption onto MPB: (a) pseudo-first-order (PFO) model, and (b) pseudo-second-order (PSO) model

Table 5 – Parameters of PFO and PSO models of adsorption kinetics for MPB

	(PFO)			(PSO)			Ref.
	k_1 / l min^{-1}	q_e / mg g^{-1}	R^2	k_2 / g mg^{-1} min^{-1}	q_e / mg g^{-1}	R^2	
Th(IV)	0.22	1.25	0.93	0.09	10.99	0.99	this work
Cr(III)	0.51	20.52	0.72	0.04	21.69	0.99	57
Ni(II)	3.13	9.05	0.53	0.76	9.28	0.93	57
Cu	0.14	0.36	0.99	0.24	0.53	0.99	17
Zn	0.05	0.41	0.97	0.06	0.44	0.93	14
V(vanadium)	0.34	8.20	0.79	0.01	8.46	0.93	12

ing its suitability for simulating adsorption kinetics.[58] The comparison results confirm that the PSO model is broadly applicable to various heavy metal adsorption processes.

3.8 Adsorption isotherms

Understanding adsorbate-adsorbent interactions requires adsorption isotherms. Mathematical models obtained from isotherm analysis are essential for understanding, designing, and optimising adsorption processes.[59] They provide insights into the extent of adsorbate build-up on the adsorbent surface under stable temperature conditions and assist in determining adsorption capacity under specific operating settings. Therefore, the results of experiments were evaluated using three isotherm models.

The Langmuir isotherm model posits that a monolayer of adsorbate molecules is formed on the adsorbent surface including identical, limited sites. It assists in establishing the maximum capacity for adsorption provided by the adsorbent.[23] Mathematically, it is expressed as:

$$q_e = \frac{q_m K_L c_e}{1 + K_L c_e} \tag{7}$$

where q_e is the equilibrium adsorption capacity (mg g^{-1}), q_m is the maximum monolayer capacity (mg g^{-1}), K_L is the Langmuir constant indicating binding affinity (l mg^{-1}), and c_e is the equilibrium concentration of the adsorbate (mg l^{-1}) [59]. The linearised form is:

$$\frac{c_e}{q_e} = \frac{1}{K_L q_m} + \frac{1}{q_m} c_e \tag{8}$$

The constant K_L and the q_m value were obtained from the linear plot of c_e / q_e *vs.* c_e (Fig. 11). The Langmuir isotherm includes a dimensionless equilibrium constant, referred to as the separation factor R_L, which can be expressed as:

$$R_L = \frac{1}{1 + K_L c_o} \tag{9}$$

where c_o is initial adsorbate concentration. The characteristics of the adsorption process are indicated by R_L value, where R_L values: 0 (irreversible), 0 to 1 (favourable), 1 (linear), and larger than 1 (unfavourable).[22]

The Freundlich isotherm model characterises adsorption on a heterogeneous surface, permitting multilayer devel-

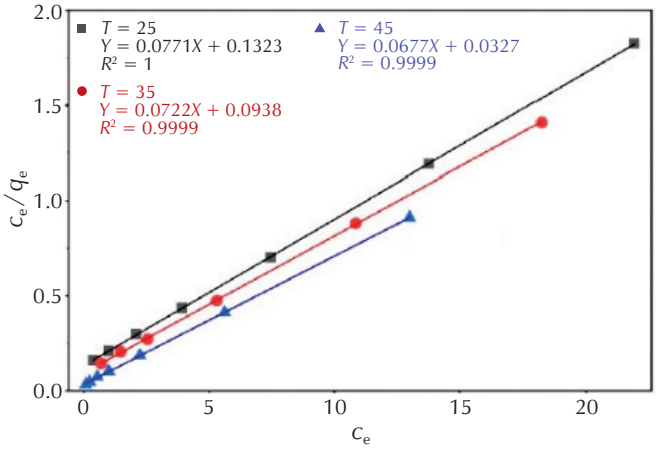

Fig. 11 – Langmuir model for the MPB adsorption

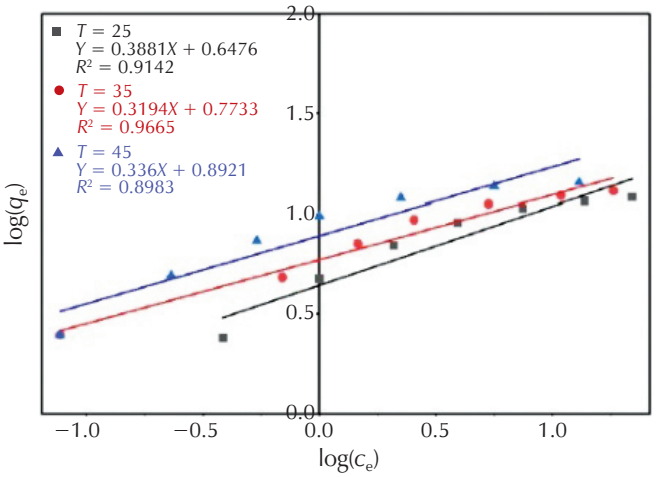

Fig. 12 – Freundlich model for the MPB adsorption

opment.[22] It is mainly used for adsorption at different concentrations and is linearly represented as:

$$\log(q_e) = \log(K_F) + \frac{1}{n}\log(c_e) \tag{10}$$

In this context, K_F (mg g^{-1}): Freundlich constant indicative of the adsorption capacity, and n: heterogeneity factor, are constants derived from the Freundlich isotherm. Values of n greater than 1 indicate a favourable adsorption process. These constants were determined by plotting log q_e against logc_e (Fig. 12) [56].

The Dubinin–Radushkevich (D–R) isotherm model clarifies the process of adsorption on microporous materials and offers insights into adsorption energy,[2] while distinguishing between chemical and physical adsorption.[58] The linear representation of the model is:

$$\ln(q_e) = \ln(q_{max}) - \beta\varepsilon^2 \tag{11}$$

where β is the mean adsorption energy constant, and q_{max} is the maximum adsorption capacity. These parameters

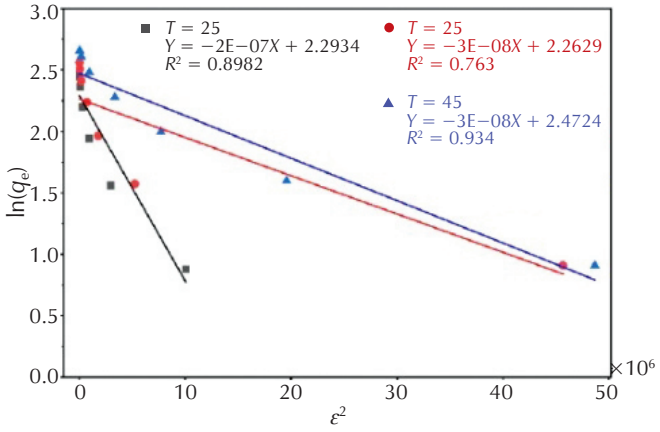

Fig. 13 – Dubinin–Radushkevich (D–R) isotherm model for Th(IV) adsorption onto modified pine bark (MPB)

were obtained from the plot of ln(q_e) against ε^2 (Fig. 14). The calculation of the ε (Polanyi potential) is performed using the following method:

$$\varepsilon = RT\ln\left(1+\frac{1}{c_e}\right) \tag{12}$$

where R (kJ K^{-1} mol^{-1}) is the universal gas constant, T is the temperature in Kelvin.

ε is the mean amount of adsorption energy determined using the following equation:

$$\varepsilon = (2\beta)^{-0.5} \tag{13}$$

The value of ε gives a detailed understanding of the process of adsorption, allowing for differentiation between chemical and physical adsorption.[60]

Table 6 – Langmuir, Freundlich, and D-R isotherm parameters for Th(IV)ions

Models	Parameters	Temperature		
		25°	35°	45°
Langmuir	q_{max}/mg g^{-1}	12.97	13.85	14.77
	K_L/mg g^{-1}	0.58	0.77	2.07
	R_L/mg g^{-1}	0.033	0.025	0.01
	R^2	1	0.999	0.999
Freundlich	K_f/l mg^{-1}	4.44	5.93	7.80
	n	2.58	3.13	2.98
	R^2	0.914	0.967	0.898
D–R	q_{max}/mg g^{-1}	9.91	12.36	11.85
	β/mol^2 kJ^{-2}	2.00E-7	3.00E-7	3.00E-8
	R^2	0.898	0.971	0.934
	E/kJ mol^{-1}	1.581	1.291	4.083

Table 7 – Th(IV) adsorption capacities q_m comparison among selected adsorbents

Adsorbent	q_{max} / mg g^{-1}	pH	T / °C	Ref.
Moringa oleifera bark	5.46	4	25°	41
Phosphorylated Schiff base (PZMP)	370.0	3.5	25°	51
silica nanoparticles	5.35	3	25°	5
Magnetic ion-imprinted chitosan resin (MICR)	14.71	3	25°	61
Manganese ferrite ($MnFe_2O_4$)	13.51	3	25°	23
nano-Kaolin/$MnFe_2O_4$	27.10	3	30°	22
Kaolinate	32.02	3	25°	22
Perlite	606.6	4.5	25°	2
Zeolite	17.0	3	25°	53

Table 6 shows that the Langmuir model demonstrated the highest accuracy in describing the experimental data, with R^2 values close to 1. This indicates that the adsorption mechanism primarily involved monolayer coverage on a uniform surface. The q_m increased with temperature, rising from (12.97 mg g^{-1} at 25 °C) to (14.77 mg g^{-1} at 45 °C). The separation factor (R_L) values, all less than 0.05, indicated a highly favourable adsorption process. In Table 7, the q_m of Th(IV) ions using different adsorbents is presented.

The Freundlich model adequately represented the data, indicating a level of surface heterogeneity, with n values higher than 1, suggesting favourable adsorption. However, the lower R^2 values relative to Langmuir indicated a less accurate fit. The D–R model study indicated that the adsorption energies (E) were below 8 kJ mol^{-1}, suggesting that the adsorption of Th(IV) onto the composite predominantly adhered to a physical adsorption (physisorption) process. Furthermore, the D–R model exhibited reduced maximum adsorption capacity (q_{max}) values relative to those derived from the Langmuir isotherm, indicating a constrained micropore packing ability of the MPB. This indicates that the adsorption process is more accurately described as monolayer adsorption onto a heterogeneous surface rather than by a purely occupancy-based mechanism. Additionally, thermodynamic analysis confirmed that the adsorption process is endothermic, whereas the Langmuir model yielded optimal match for equilibrium data.[62]

3.9 Thermodynamics of the adsorption process

The fundamental features of the adsorption process were elucidated by measuring thermodynamic parameters, $\Delta G°$ (Gibbs free energy change), $\Delta H°$ (enthalpy change), and $\Delta S°$ (entropy change).[25] The subsequent thermodynamic equations were used:

$$\Delta G^{\circ} = -RT\ln(K_d) \tag{14}$$

$$\ln(K_d) = \frac{\Delta S^{\circ}}{R} - \frac{\Delta H^{\circ}}{RT} \tag{15}$$

In Eq. (14), K_d is the thermodynamic distribution coefficient, T is the temperature measured in Kelvin, and R is the universal gas constant (8.3145 J mol^{-1} K^{-1}).[53]

The value of $\ln(K_d)$ was derived from the intercept of the linear graph plotting $\ln(q_e/c_e)$ against q_e, as illustrated in Fig. 14. These parameters explain the spontaneity and thermal variation linked with the adsorption process.[23] The values $\Delta H°$ and $\Delta S°$ were obtained using the slope and intercept of the $\ln(K_d)$ against $1/T$, as illustrated in Fig. 15 and Table 8.

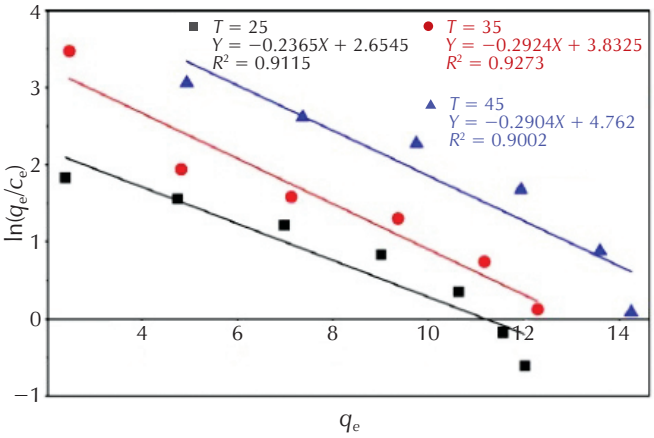

Fig. 14 – Th(IV) isotherms of adsorption on MPB at different temperatures

Table 8 – Distribution coefficient (K_d) at different temperatures for Th(IV)

$1/T$	$\ln(K_d)$	K_d
0.0034	2.65	14.22
0.0032	3.82	46.18
0.0031	4.76	116.98

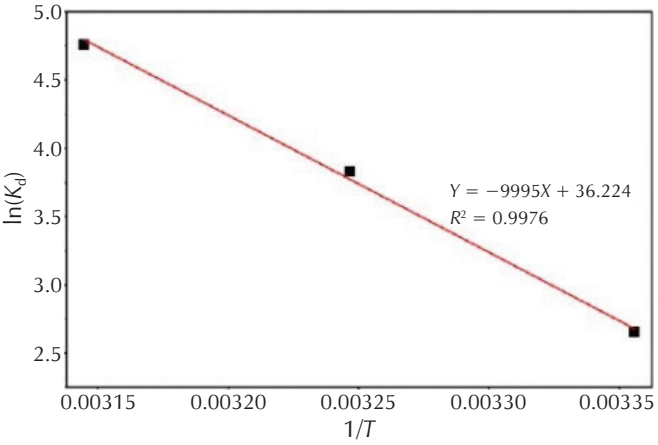

Fig. 15 – Thermodynamics of adsorption Th(IV) by MPB

Table 9 – Thermodynamic parameters ($\Delta G°$, $\Delta H°$, $\Delta S°$) for Th(IV) adsorption at 25 °C

	$\Delta G°$ / kJ mol^{-1}	$\Delta H°$ / kJ mol^{-1}	$\Delta S°$ / J mol^{-1} K^{-1}
Th(IV)	−6.58	83.10	301.18

Table 9 demonstrates that the Gibbs free energy ($\Delta G°$) for Th(IV) adsorption onto modified pine bark (MPB) was negative across all tested temperatures, indicating that the process was thermodynamically favourable and spontaneous. The positive enthalpy $\Delta H°$ implies an endothermic adsorption process, while the positive entropy $\Delta S°$ means an increase in randomness at the interface between the solid and the liquid during adsorption, suggesting a more stable and disordered configuration of Th(IV) ions on the MPB surface.

3.10 Reusability and stability of MPB adsorbent

The reusability of MPB was evaluated via batch desorption tests. Th(IV) ions were initially adsorbed on MPB surface and subsequently desorbed over three successive cycles. Two filtrates were used: 0.10 M HNO_3 and 1 M HNO_3. The findings demonstrated that the maximum desorption rate of 82.8 % was attained with 0.10 M HNO_3, whereas 1 M HNO_3 provided 74.0 % under the same conditions. The results confirm that MPB can be efficiently regenerated and reused through several adsorption-desorption cycles for the extraction of Th(IV) from water.

4 Conclusion

This research demonstrates the successful modification of pine bark using hydrochloric acid. The physicochemical properties of MPB were characterised using FTIR, XRD, SEM, BET, and ICP analyses. The adsorption behaviour of Th(IV) on MPB was examined under varying conditions. The results show that adsorption efficiency was strongly influenced by operational parameters such as temperature, pH, contact time, and adsorbent dosage. MPB exhibited enhanced adsorption capabilities, achieving a maximum q_m of 12.97. The good agreement with the PSO model suggests that the adsorption process may involve interactions between adsorbate and adsorbent. However, this alone does not conclusively indicate chemisorption.

The low D–R mean adsorption energy ($E < 8$ kJ mol^{-1}) indicates that the process is predominantly governed by physisorption, although contributions from other interactions cannot be excluded. Thermodynamic analysis revealed negative values of $\Delta G°$, confirming the spontaneous and favourable nature of the adsorption process. The positive values of $\Delta S°$ and $\Delta H°$ confirm the endothermic nature of the process and the increase in disorder at the solid–liquid interfaces. A distribution coefficient (K_d) of 116.98 at 45 °C was obtained for MPB, demonstrating its effectiveness in the remediation of Th(IV) from water.

List of abbreviations
Popis kratica

MPB – modified pine bark
PB – pine bark
WHO – World Health Organization
EPA – Environmental Protection Agency
MCL – maximum contaminant level
FTIR – Fourier transform infrared spectroscopy
XRD – X-ray diffraction
BET – Brunauer–Emmett–Teller
DFT – density functional theory
SEM – scanning electron microscopy
EDX – energy-dispersive X-ray spectroscopy
ICP-OES – inductively coupled plasma – optical emission spectroscopy
ICP-MS – inductively coupled plasma – mass spectrometry
PFO – pseudo-first-order
PSO – pseudo-second-order
D–R – Dubinin–Radushkevich

References
Literatura

1. *K. Pyrzynska,* Removal of cadmium from wastewaters with low-cost adsorbents, J. Environ. Chem. Eng. **7** (2019) 102795, doi: https://doi.org/10.1016/j.jece.2018.11.040.
2. *Z. Talip, M. Eral, Ü. Hiçsönmez,* Adsorption of thorium from aqueous solutions by perlite, J. Environ. Radioact. **100** (2009) 139–143, doi: https://doi.org/10.1016/j.jenvrad.2008.09.004.
3. *V. K. Gupta, Suhas,* Application of low-cost adsorbents for dye removal – A review, J. Environ. Manage. **90** (2009) 2313–2342, doi: https://doi.org/10.1016/j.jenvman.2008.11.017.
4. *Y. Huang, H. Zheng, H. Li, Z. Zhang, C. Zhao, Q. Gou, Y. Liu,* Highly effective and selective adsorption of thorium(IV) from aqueous solution using mesoporous graphite carbon nitride prepared by sol–gel template method, Chem. Eng. J. **410** (2021) 128321, doi: https://doi.org/10.1016/j.cej.2020.128321.
5. *L. S. Ismail, F. I. Khalili, F. M. Abu Orabi,* Thorium(IV) removal and recovery from aqueous solutions using modified silica nanoparticles with cysteine or methionine amino acids, Desalin. Water Treat. **196** (2020) 161–176, doi: https://doi.org/10.5004/dwt.2020.25936.
6. *A. Y. Zahrim,* Current progress on removal of recalcitrance coloured particles from anaerobically treated effluent using coagulation–flocculation, Vol. 2018, pp. 149–163, doi: https://doi.org/10.1007/978-981-10-8129-3_9.
7. *S.-K. Jiang, X.-Y. Chao, C.-X. Zhang, Q. Shi, Z.-Y. Wang, M.-L. Liu, S.-P. Sun,* Removing miscellaneous heavy metals by all-in-one ion exchange–nanofiltration membrane, Water Res. **222** (2022) 118888, doi: https://doi.org/10.1016/j.watres.2022.118888.
8. *L. Li, Y. Zhang, Y. Pan, M. Ni, W. Yang, Y. Huang,* Phosphorus absorption and release in biofilm sequencing batch reactor: The combined action of cells and extracellular polymeric substances and the characteristics of polymer metabolism,

J. Water Process Eng. **49** (2022) 102979, doi: https://doi.org/10.1016/j.jwpe.2022.102979.

9. *R. R. Solís, M. A. Quintana, G. Blázquez, M. Calero, M. J. Muñoz-Batista*, Ruthenium deposited onto graphitic carbon modified with boron for the intensified photocatalytic production of benzaldehyde, Catal. Today **423** (2023) 114266, doi: https://doi.org/10.1016/j.cattod.2023.114266.
10. *W. Liu, Y. Huang, G. Huang, L. Fan, Y. Xie, Q. Zhang, J. Shi,* Facile strategy to separate uranium(VI) using glued amidoxime-functionalized composite beads synthesized from aqueous solution, Sep. Purif. Technol. **293** (2022) 121132, doi: https://doi.org/10.1016/j.seppur.2022.121132.
11. *B. Volesky,* Biosorption and me, Water Res. **41** (2007) 4017–4029, doi: https://doi.org/10.1016/j.watres.2007.05.062.
12. *R. Zhang, T. Leiviskä,* Surface modification of pine bark with quaternary ammonium groups and its use for vanadium removal, Chem. Eng. J. **385** (2020) 123967, doi: https://doi.org/10.1016/j.cej.2019.123967.
13. *G. Mukherjee, S. Dhiman,* Waste Management, CRC Press, Boca Raton, 2022, doi: https://doi.org/10.1201/9780429341106.
14. *M. Oh, M. A. Tshabalala,* Pelletized ponderosa pine bark for adsorption of toxic heavy metals from water, BioResources **2** (2007) 66–81, doi: https://doi.org/10.15376/biores.2.1.66-81.
15. *K. Philippou, I. Anastopoulos, I. Pashalidis, A. Hosseini-Bandegharaei, M. Usman, M. Kornaros, M. Omirou, D. Kalderis, J. V. Milojković, Z. R. Lopičić, M. Abatal,* The application of pine-based adsorbents to remove potentially toxic elements from aqueous solutions, in: Sorbent Materials for Controlling Environmental Pollution, Elsevier, 2021, pp. 113–133, doi: https://doi.org/10.1016/B978-0-12-820042-1.00016-X.
16. *S. Al-Asheh, Z. Duvnjak,* Sorption of cadmium and other heavy metals by pine bark, J. Hazard. Mater. **56** (1997) 35–51, doi: https://doi.org/10.1016/S0304-3894(97)00040-X.
17. *S. Wierzba, A. Doihanczuk-Środka, J. Kníž,* Optimization of the sorption process of copper cations from aqueous solution by pine bark *(Pinus sylvestris),* Desalin. Water Treat. **186** (2020) 258–266, doi: https://doi.org/10.5004/dwt.2020.25626.
18. *J. Ghosh, N. S. Rupanty, F. Khan, T. Noor, R. Jahangir, S. Mirmohammadsadeghi, T. Islam,* Grafting modification for textile functionalization: innovations and applications, Discover Appl. Sci. **7** (2025) 49, doi: https://doi.org/10.1007/s42452-024-06364-5.
19. *P. Bhattacharya, A. H. Welch, K. M. Ahmed, G. Jacks, R. Naidu,* Arsenic in groundwater of sedimentary aquifers, Appl. Geochem. **19** (2004) 163–167, doi: https://doi.org/10.1016/j.apgeochem.2003.09.004.
20. *G. Blázquez, M. A. Martín-Lara, E. Dionisio-Ruiz, G. Tenorio, M. Calero,* Evaluation and comparison of the biosorption process of copper ions onto olive stone and pine bark, J. Ind. Eng. Chem. **17** (2011) 824–833, doi: https://doi.org/10.1016/j.jiec.2011.08.003.
21. *B. Wang, T. Wu, S. Angaiah, V. Murugadoss, J.-E. Ryu, E. K. Wujcik, N. Lu, D. P. Young, Q. Gao, Z. Guo,* Development of nanocomposite adsorbents for heavy metal removal from wastewater, ES Mater. Manuf. **2** (2018) 35–44, doi: https://doi.org/10.30919/esmm5f175.
22. *J. Jaaferh, F. I. Khalili, A. S. Masadeh,* Removal of Th(IV) from groundwater by adsorption onto nano-kaolin and nano-kaolin/$MnFe_2O_4$ composite, Int. J. Environ. Anal. Chem. **105** (2025) 458–480, doi: https://doi.org/10.1080/03067319.2023.2263385.
23. *M. Alaqarbeh, F. I. Khalili, O. Kanoun,* Manganese ferrite ($MnFe_2O_4$) as potential nanosorbent for adsorption of uranium(VI) and thorium(IV), J. Radioanal. Nucl. Chem. **323** (2020) 515–537, doi: https://doi.org/10.1007/s10967-019-06953-4.
24. *J. M. Aljaafreh, K. A. Wahab Al harahsheh, F. I. Khalili, A. Masadeh, M. S. Mousa, O. A. Alnasra, A. I. Abushawer, A. M Abuamr,* Enhancing U(VI) removal from water using nano-kaolin and nano-kaolin/$MnFe_2O_4$ composite adsorbents, Phys. Scr. **100** (2025) 085411, doi: https://doi.org/10.1088/1402-4896/adf602.
25. *J. Wang, X. Guo,* Adsorption kinetics and isotherm models of heavy metals by various adsorbents: An overview, Crit. Rev. Environ. Sci. Technol. **53** (2023) 1837–1865, doi: https://doi.org/10.1080/10643389.2023.2221157.
26. *H. Musa, O. Alnasra, F. Khalili,* Innovative study on the removal of thorium(IV) and uranium(VI) ions from aqueous solutions via oak-derived charcoal: kinetic analysis and adsorptive performance, J. Radioanal. Nucl. Chem. (2025), doi: https://doi.org/10.1007/s10967-025-10177-0.
27. *S. P. Mun, C. S. Ku, J. P. Kim,* Adsorption of metal and uranyl ions onto amidoximated *Pinus densiflora* bark, Wood Sci. Technol. **44** (2010) 283–299, doi: https://doi.org/10.1007/s00226-009-0276-z.
28. *A. L. Arim, D. F. M. Cecílio, M. J. Quina, L.M . Gando-Ferreira*, Development and characterization of pine bark with enhanced capacity for uptaking Cr(III) from aqueous solutions, Can. J. Chem. Eng. **96** (2018) 855–864, doi: https://doi.org/10.1002/cjce.23029.
29. *M. E. Argun, S. Dursun, M. Karatas,* Removal of Cd(II), Pb(II), Cu(II) and Ni(II) from water using modified pine bark, Desalination **249** (2009) 519–527, doi: https://doi.org/10.1016/j.desal.2009.01.020.
30. *A. Şen, H. Pereira, M. A. Olivella, I. Villaescusa,* Heavy metals removal in aqueous environments using bark as a biosorbent, Int. J. Environ. Sci. Technol. **12** (2015) 391–404, doi: https://doi.org/10.1007/s13762-014-0525-z.
31. *N. Gama, A. Ferreira, A. Barros-Timmons, D. Evtuguin,* Polyamide 6/modified pine bark particle composites for additive manufacturing, J. Mater. Sci. **56** (2021) 19093–19105, doi: https://doi.org/10.1007/s10853-021-06443-7.
32. *D. Schwantes, A. C. Gonçalves Jr., M. A. Campagnolo, C. R. T. Tarley, D. C. Dragunski, A. de Varennes, A. K. dos Santos Silva, E. Conradi Junior,* Chemical modifications on *Pinus* bark for adsorption of toxic metals, J. Environ. Chem. Eng. **6** (2018) 1271–1278, doi: https://doi.org/10.1016/j.jece.2018.01.044.
33. *K. Litefti, M. S. Freire, M. Stitou, J. González-Álvarez,* Adsorption of an anionic dye (Congo red) from aqueous solutions by pine bark, Sci. Rep. **9** (2019) 16530, doi: https://doi.org/10.1038/s41598-019-53046-z.
34. *M. Traoré, J. Kaal, A. Martínez Cortizas*, Differentiation between pine woods according to species and growing location using FTIR-ATR, Wood Sci. Technol. **52** (2018) 487–504, doi: https://doi.org/10.1007/s00226-017-0967-9.
35. *S. I. Tsyganova, G. N. Bondarenko, O. Y. Fetisova,* Energy storage in carbon materials synthesized from fir bark modified with graphite and zinc chloride, Wood Sci. Technol. **55** (2021) 1123–1134, doi: https://doi.org/10.1007/s00226-021-01298-2.
36. *Z. Wang, W. Xu, F. Jie, Z. Zhao, K. Zhou, H. Liu,* The selective adsorption performance and mechanism of multiwall magnetic carbon nanotubes for heavy metals in wastewater, Sci. Rep. **11** (2021) 16878, doi: https://doi.org/10.1038/s41598-021-96465-7.
37. *D. Barros, É. Fernandes, M. Jesus, L. Barros, J. I. Alonso-Esteban, P. Pires, M. Vaz Velho,* The chemical characterisation

of the maritime pine bark cultivated in Northern Portugal, Plants **12** (2023) 3940, doi: https://doi.org/10.3390/plants12233940.

38. *I. Brás, L.T. Lemos, A. Alves, M. F. R. Pereira,* Application of pine bark as a sorbent for organic pollutants in effluents, Manag. Environ. Qual. **15** (2004) 491–501, doi: https://doi.org/10.1108/14777830410553933.
39. *Y. Han, M. Yu, L. Wang,* Bio-based films prepared with soybean by-products and pine (*Pinus densiflora*) bark extract, J. Clean. Prod. **187** (2018) 1–8, doi: https://doi.org/10.1016/j.jclepro.2018.03.115.
40. *S. I. Tsyganova, N. G. Maximov, E. V. Masurova, O. Y. Fetisova, O. P Taran,* Study of the synthesis of carbon-containing materials based on modified pine bark for the accumulation of electric charge, Wood Sci. Technol. **57** (2023) 135–146, doi: https://doi.org/10.1007/s00226-022-01438-2.
41. *A. A. Jangher, B. M. Mahara, S. W. Al-Rmalli,* Biosorption of thorium from aqueous solutions by *Moringa oleifera* bark: equilibrium and kinetic studies, J. Appl. Chem. Sci. Int. **8** (2017) 22–31.
42. *G. Montes-Atenas, S. L. M. Schroeder,* Sustainable natural adsorbents for heavy metal removal from wastewater: lead sorption on pine bark (*Pinus radiata* D. Don), Surf. Interface Anal. **47** (2015) 996–1000, doi: https://doi.org/10.1002/sia.5807.
43. *R. Feria-Reyes, S. O. Ramírez-Cruz, F. Ruiz-Aquino, L. H. Robledo-Taboada, M. A. Sánchez-Medina, O. F. Mijangos-Ricárdez, R. Gabriel-Parra, M. E. Suárez-Mota, R. Puc-Kauil, J. Porcallo-Vargas,* Pine bark as a potential source of condensed tannin: analysis through Fourier transform infrared spectroscopy (FTIR), scanning electron microscopy (SEM), and energy dispersive X-ray (EDX), Forests **14** (2023) 1433, doi: https://doi.org/10.3390/f14071433.
44. *J. Routa, H. Brännström, J. Hellström, J. Laitila,* Influence of storage on the physical and chemical properties of Scots pine bark, Bioenergy Res. **14** (2021) 575–587, doi: https://doi.org/10.1007/s12155-020-10206-8.
45. *M. Mohammadzadeh, T. Leiviskä,* Iron-modified peat and magnetite–pine bark biosorbents for levofloxacin and trimethoprim removal from synthetic water and various pharmaceuticals from real wastewater, Ind. Crops Prod. **195** (2023) 116491, doi: https://doi.org/10.1016/j.indcrop.2023.116491.
46. *J. Y. Kim, J. Park, J. Choi, J. Kim,* Determination of metal concentration in road-side trees from an industrial area using laser ablation inductively coupled plasma mass spectrometry, Minerals **10** (2020) 175, doi: https://doi.org/10.3390/min10020175.
47. *A. Anca-Couce, N. Zobel, A. Berger, F. Behrendt,* Smouldering of pine wood: kinetics and reaction heats, Combust. Flame **159** (2012) 1708–1719, doi: https://doi.org/10.1016/j.combustflame.2011.11.015.
48. *V. Kamar, R. Dagalp, M. Taştekin,* Determination of heavy metals in almonds and mistletoe as a parasite growing on the almond tree using ICP-OES or ICP-MS, Biol. Trace Elem. Res. **185** (2018) 226–235, doi: https://doi.org/10.1007/s12011-017-1223-8.
49. *Y. Ni, W. Bu, X. Ding, K. Xiong, H. Wang, C. Yang, S. Hu, W. Men,* Automated method for concurrent determination of thorium (^{230}Th, ^{232}Th) and uranium (^{234}U, ^{235}U, ^{238}U) isotopes in water matrices with ICP-MS/MS, J. Anal. At. Spectrom. **37** (2022) 919–928, doi: https://doi.org/10.1039/D1JA00450F.
50. *J. Jaaferh, F. I. Khalili, A. S. Masadeh*, Removal of Th(IV) from groundwater by adsorption onto nano-kaolin and nano-kaolin/$MnFe_2O_4$ composite, Int. J. Environ. Anal. Chem. (2023) 1–23, doi: https://doi.org/10.1080/03067319.2023.2263385
51. *M. A. Gado*, Efficient adsorption of thorium and cerium from Rosetta monazite concentrate using a novel phosphorylated Schiff-base adsorbent, J. Radioanal. Nucl. Chem. **333** (2024) 5025–5048, doi: https://doi.org/10.1007/s10967-024-09667-4.
52. *M. Jiang, Q. Wang, X. Jin, Z. Chen,* Removal of Pb(II) from aqueous solution using modified and unmodified kaolinite clay, J. Hazard. Mater. **170** (2009) 332–339, doi: https://doi.org/10.1016/j.jhazmat.2009.04.092.
53. *M. Al-Shaybe, F. Khalili,* Adsorption of thorium(IV) and uranium(VI) by Tulul al-Shabba zeolitic tuff, Jordan, Jordan J. Earth Environ. Sci. **2** (2009) 109–119.
54. *Z. Raji, A. Karim, A. Karam, S. Khalloufi,* Adsorption of heavy metals: mechanisms, kinetics, and applications of various adsorbents in wastewater remediation – A review, Waste **1** (2023) 775–805, doi: https://doi.org/10.3390/waste1030046.
55. *K. G. Akpomie, J. Conradie, K. A. Adegoke, K. O. Oyedotun, J. O. Ighalo, J. F. Amaku, C. Olisah, A. O. Adeola, K. O. Iwuozor ,* Adsorption mechanism and modeling of radionuclides and heavy metals onto ZnO nanoparticles: a review, Appl. Water Sci. **13** (2023) 20, doi: https://doi.org/10.1007/s13201-022-01827-9.
56. *M. Paredes-Laverde, J. A. Cárdenas-Jiménez, J. Porras, N. Acelas, R. A. Torres-Palma,* Green adsorbents for pharmaceutics removal from urine: analysis of isotherms, kinetics, adsorption interactions, cost estimation, and environmental impact, J. Environ. Manage. **368** (2024) 122162, doi: https://doi.org/10.1016/j.jenvman.2024.122162.
57. *A. L. Arim, G. Guzzo, M. J. Quina, L. M. Gando-Ferreira,* Single and binary sorption of Cr(III) and Ni(II) onto modified pine bark, Environ. Sci. Pollut. Res. **25** (2018) 28039–28049, doi: https://doi.org/10.1007/s11356-018-2843-z.
58. *O. Alnasra, M. Alkhabbas, F. Khalili, D. Abdel Jabbar,* Exploring the adsorptive behavior of U(VI) ions on avocado seed-derived activated carbon: an in-depth kinetic and thermodynamic analysis, J. Radioanal. Nucl. Chem. **334** (2025) 1741–1755, doi: https://doi.org/10.1007/s10967-024-09972-y.
59. *R. A. M. Issa, A. O. El Amari, H. B. Al Hanash, H. M. Etmimi,* Removal of uranium (VI) ion from aqueous solution using kaolinite, Kuwait J. Sci. **50** (2023) 609–614, doi: https://doi.org/10.1016/j.kjs.2023.03.010.
60. *R. González-Feijoo, V. Santás-Miguel, D. Arenas-Lago, E. Álvarez-Rodríguez, A. Núñez-Delgado, M. Arias-Estévez, P. Pérez-Rodríguez,* Effectiveness of cork and pine bark powders as biosorbents for potentially toxic elements present in aqueous solution, Environ. Res. **250** (2024) 118455, doi: https://doi.org/10.1016/j.envres.2024.118455.
61. *G. Huang, Z. Chen, L. Wang, T. Lv, J. Shi,* Removal of thorium(IV) from aqueous solution using magnetic ion-imprinted chitosan resin, J. Radioanal. Nucl. Chem. **310** (2016) 1265–1272, doi: https://doi.org/10.1007/s10967-016-4993-0.
62. *H. K. Boparai, M. Joseph, D. M. O'Carroll,* Kinetics and thermodynamics of cadmium ion removal by adsorption onto nano zerovalent iron particles, J. Hazard. Mater. **186** (2011) 458–465, doi: https://doi.org/10.1016/j.jhazmat.2010.11.029.

SAŽETAK

Kemijski modificirana borova kora kao održiv i jeftin biosorbens za učinkovito uklanjanje Th(IV) iz vode: karakterizacija, kinetička, izoterma i termodinamička istraživanja

Jafar M. Aljaafreh,[a] *Fawwaz I. Khalili*,[b] *Marwan Suleiman Mousa*,[c] *Omar Alaa Alnasra*,[d] *Dinara Sobola*,[e] *Guo-Zhen Zhu*,[f] *Kiril Lisichkov*,[g] *Tome Kitanovski*,[g*] *Ahmad M. D. (Assa'd) Jaber*,[h] *Ziad M. Alqudah*[i] i *Adel M. Abuamr*[f]

Adsorpcijsko ponašanje torijevih iona (Th(IV)) na modificiranoj borovoj kori (MPB) sustavno je istraženo ispitivanjem utjecaja pH vrijednosti, doze adsorbensa, temperature i vremena kontakta. Kinetičkom analizom primjenom modela pseudo-drugog reda (PSO) utvrđeno je da je ravnotežni adsorpcijski kapacitet (q_e) MPB-a, pri pH 3, dosegnuo maksimalnu učinkovitost uklanjanja od približno 90 %, uz vrijednost q_e od 12,97 mg g^{-1} pri 25 °C. Analiza adsorpcijskih izotermi provedena je primjenom Langmuirova, Freundlichova i Dubinin–Radushkevicheva modela. Langmuirov model pokazao je bolju podudarnost s eksperimentalnim podacima (R^2) u odnosu na Freundlichov model, što upućuje na jednoslojnu adsorpciju uz određeni stupanj heterogenosti površine adsorbensa. Termodinamički parametri, uključujući promjenu entalpije ($\Delta H°$), entropije ($\Delta S°$) i Gibbsove slobodne energije ($\Delta G°$), određeni su pri različitim temperaturama. Pri 25 °C dobivene su vrijednosti $\Delta H° = 83{,}10$ kJ mol^{-1}, $\Delta G° = -6{,}58$ kJ mol^{-1} i $\Delta S° = 301{,}18$ J mol^{-1} K^{-1}. Dobiveni rezultati potvrđuju da je proces adsorpcije spontan i endoterman te da ga prati povećanje entropije sustava. Općenito, modificirana borova kora pokazala je značajan potencijal kao učinkovit adsorbens za uklanjanje Th(IV) iona iz vodenih otopina.

Ključne riječi
Adsorpcija, modeliranje adsorpcijskih izotermi, borova kora, modificirana borova kora, torij

[a] *Department of Physics, School of Science, The University of Jordan, Amman, Jordan*
[b] *Department of Chemistry, School of Science, The University of Jordan, Amman, Jordan*
[c] *Department of Renewable Energy Engineering, Jadara University, Irbid 21 110, Jordan*
[d] *Department of Chemistry, School of Science, Jerash Private University, Jerash, Jordan*
[e] *Department of Physics, Faculty of Electrical Engineering and Communication, Brno, University of Technology, 61 600 Brno, Češka Republika*
[f] *Department of Mechanical Engineering and Manitoba Institute for Materials, University of Manitoba, Winnipeg, MB R3T 5V6, Kanada*
[g] *Tehnološko-metalurški fakultet, Sv. Ćiril i Metod Sveučilište u Skopju, Ruger Boskovic 16, 1000 Skopje, Sjeverna Makedonija*
[h] *Department of Basic Humanities and Sciences, Faculty of Medicine, Aqaba Medical Sciences University, Aqaba 77 110, Jordan*
[i] *Jordan Atomic Energy Commission, Amman 11 934, Jordan*

Izvorni znanstveni rad
Prispjelo 3. veljače 2026.
Prihvaćeno 3. travnja 2026.